Supporting Information: Hybrid Photon-Plasmon Coupling and Ultrafast Control of Nanoantennas on a Silicon Photonic Chip

BIGENG CHEN,[1] ROMAN BRUCK,[1] DANIEL TRAVISS, [1] ALI Z. KHOKHAR,[2] SCOTT REYNOLDS,[2] DAVID J. THOMSON,[2] GORAN Z. MASHANOVICH,[2] GRAHAM T. REED,[2] AND OTTO L. MUSKENS[1,*]

[1] *Physics and Astronomy, Faculty of Physical Sciences and Engineering, University of Southampton, Southampton SO17 1BJ, UK*
[2] *Optoelectronics Research Centre, University of Southampton, Southampton SO17 1BJ, UK*
**Corresponding author: o.muskens@soton.ac.uk*

S1. Scattering from 1-5 nanoantennas on waveguides

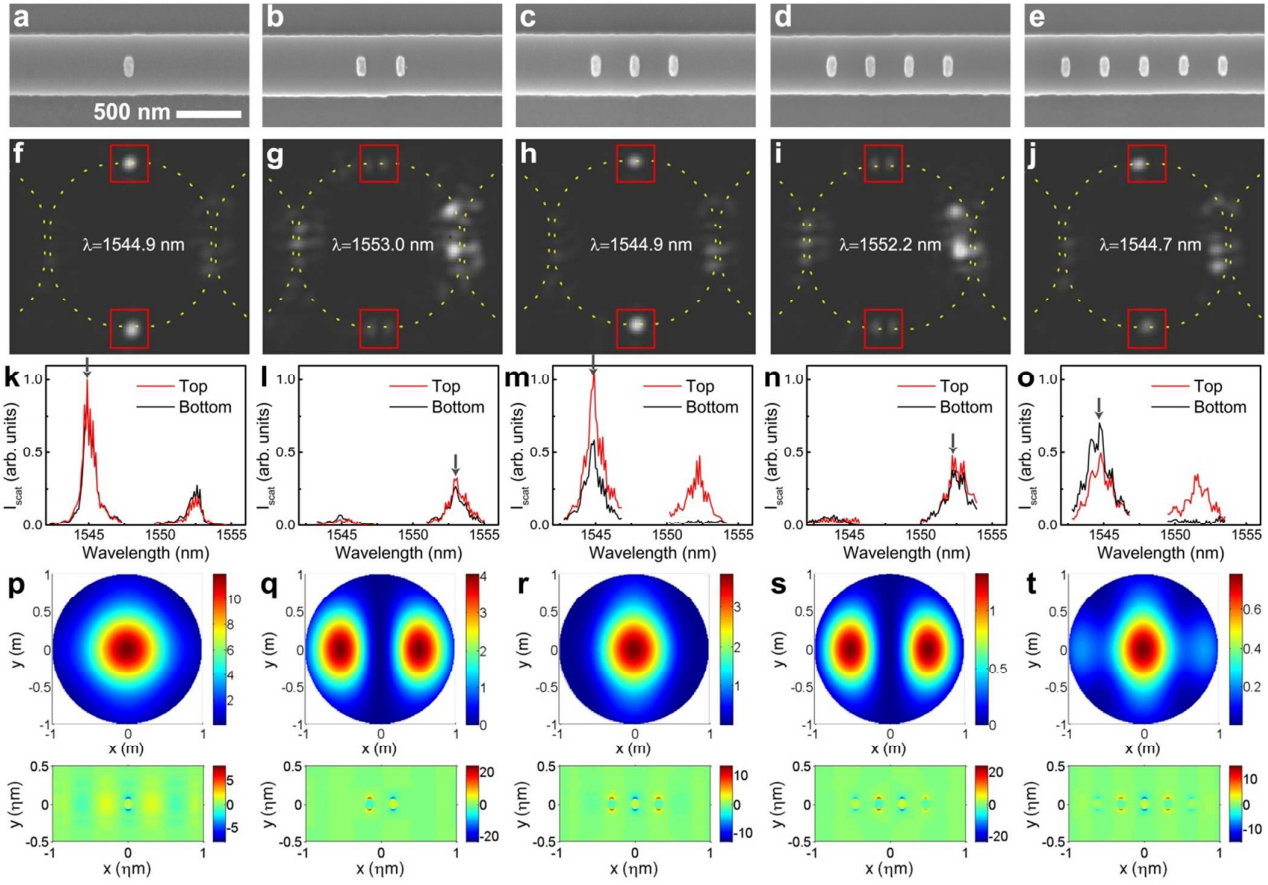

Figure S1 Scattering maps from antennas on racetrack. a-e, SEM images of top sections of racetracks with different numbers of nanoantennas varying from 1 to 5, respectively. Scale bar in the left one is applicable to the other 4 images. **f-j**, Dark-field images of the 5 racetracks transmitting suppressed modes with 1 to 5 nanoantennas on their horizontal sections, respectively. **k-o**, Measured scattering spectra from the 1- to 5-nanoantenna arrays on the racetrack. The arrows in each spectrum denote the wavelengths at which the Dark-field images in **f-j** were collected. **p-t**, Calculated far-field patterns projected from 1- to 5-nanoantenna arrays overlapping with standing wave anti-nodes in single straight waveguides and the corresponding near field E_y distributions near the antennas.

S2. Spatial maps for bottom output of the 3-nanoantenna racetrack resonator

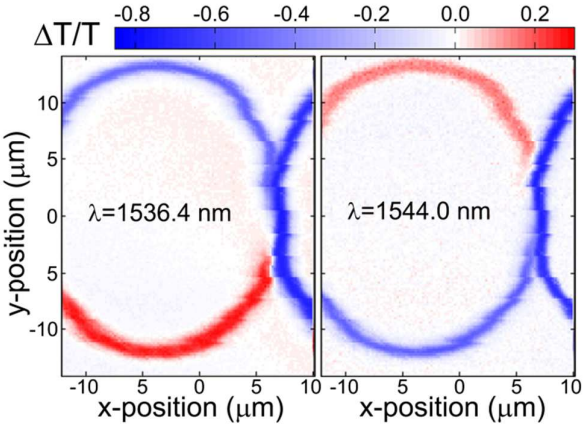

Figure S2 **Spatial photomodulation maps for bottom output. Spatial maps over the input coupler region at 5 ps delay time for bottom output at the wavelengths of 1536.4 nm and 1544.0 nm, showing the opposite polarity to the top output spatial maps in Figure 3c of the main text.**

S3. Photo-modulated output spectra of racetrack resonators with 0-5 nanoantennas and pump on top or bottom input waveguides

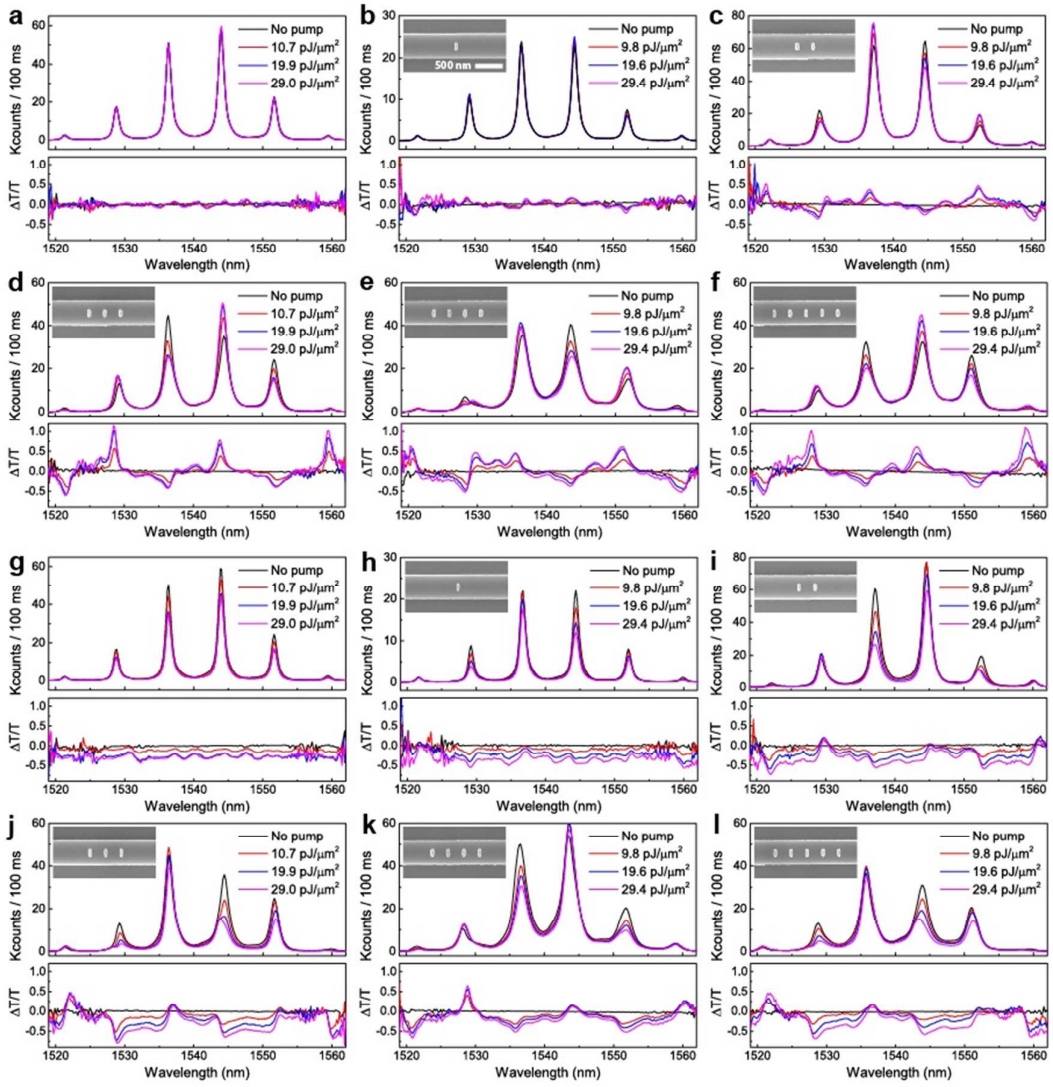

Figure S3 Direct and cross-modulation spectra for top output. a-f, Top output spectra and corresponding derided $\Delta T/T$ with pumping on the **Bottom** input waveguides at different fluence of the racetracks with 0- to 5-nanoantenna arrays. **g-l, Top** output spectra and corresponding derided $\Delta T/T$ with pumping on the **top** input waveguides at different fluence of the racetracks with 0- to 5-nanoantenna arrays. Insets: SEM images of top sections of racetracks with different numbers of nanoantennas varying from 0 to 5. Scale bar in the inset of **b** also applies to the other 9 inset SEM images.

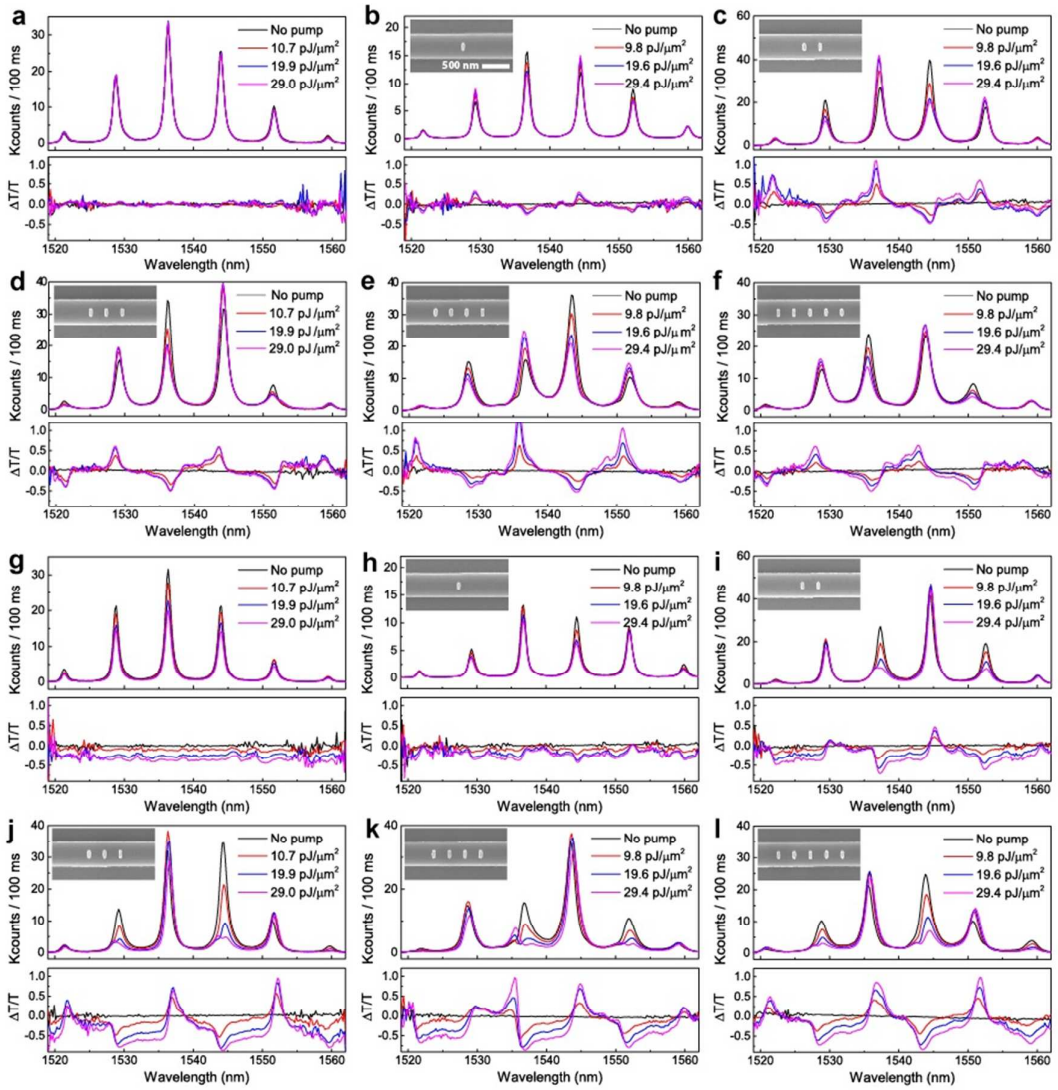

Figure S4 Direct and cross-modulation spectra for bottom output. a-**f**, **Bottom** output spectra and corresponding derided $\Delta T/T$ with pumping on the **top** input waveguides at different fluence of the racetracks with 0- to 5-nanoantenna arrays. **g**-**l**, **Bottom** output spectra and corresponding derided $\Delta T/T$ with pumping on the **bottom** input waveguides at different fluence of the racetracks with 0- to 5-nanoantenna arrays. Insets: SEM images of top sections of racetracks with different numbers of nanoantennas varying from 0 to 5. Scale bar in the inset of **b** also applies to the other 9 inset SEM images.

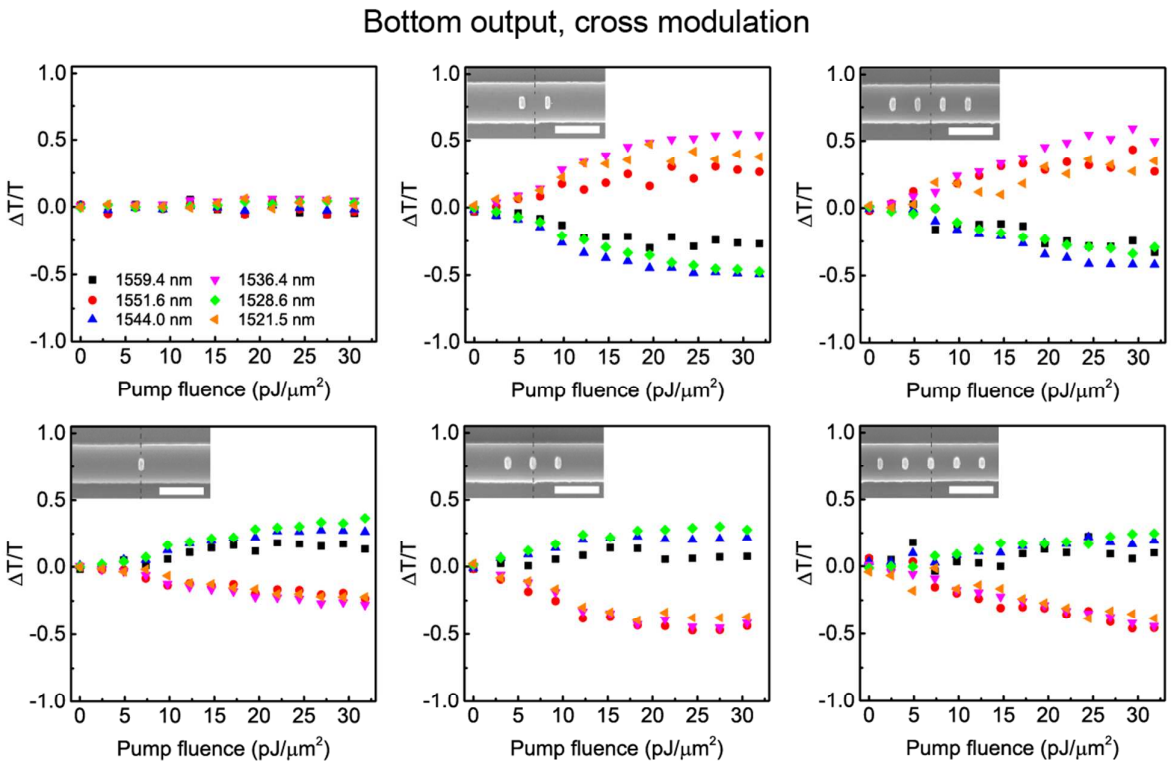

Figure S5 Modulation depth $\Delta T/T$ of racetracks with different numbers of nanoantennas, bottom outputs. Cross-modulation depths $\Delta T/T$ of bottom outputs from five racetracks which have the nanoantenna arrays with element numbers from 0 to 5. Six resonant modes are included, in which odd modes and even modes are grouped in green and red shapes, respectively. The insets show the SEM images of the nanoantennas on the racetrack around position $-L/4$ (dashed line). Scale bar, 500 nm.

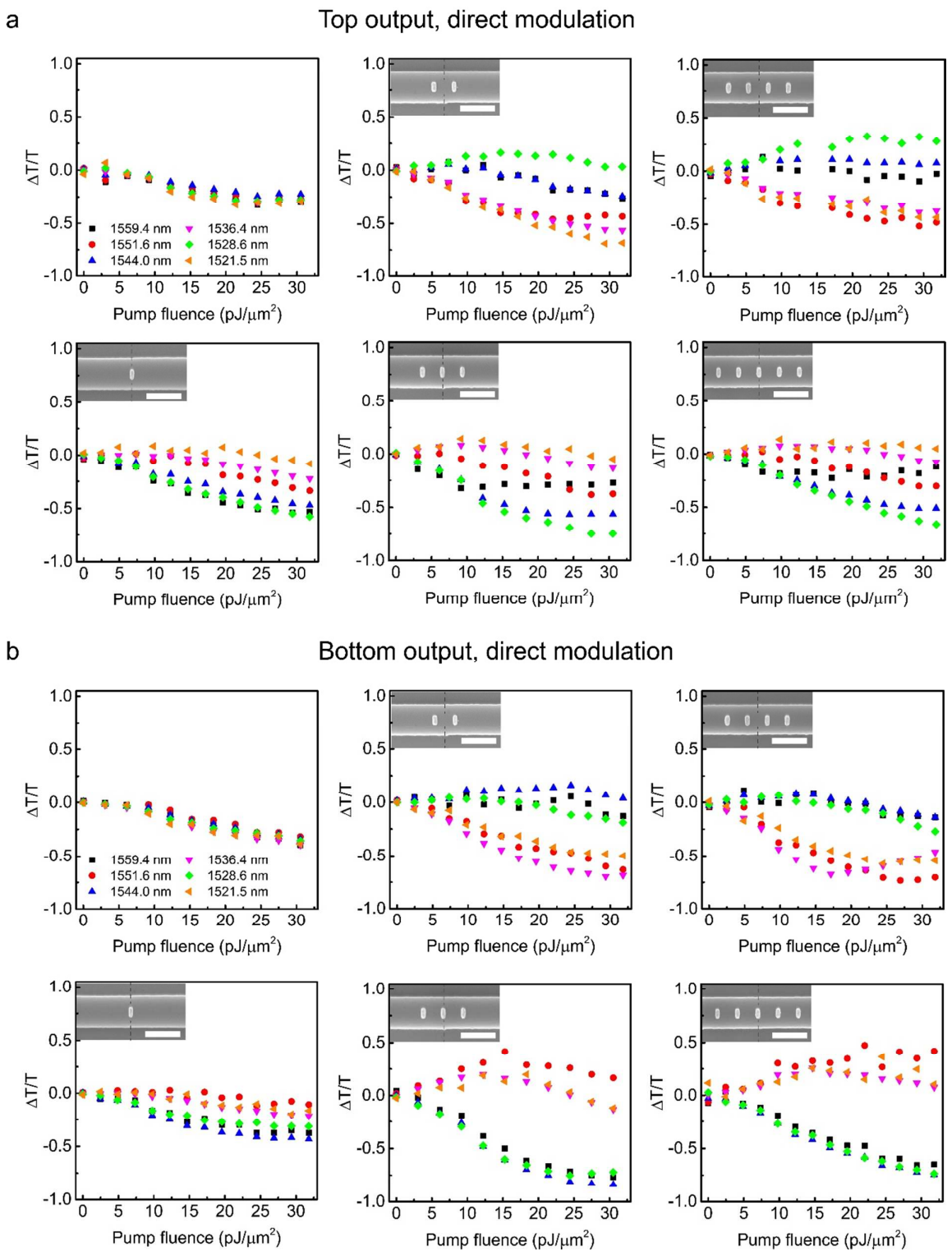

Figure S6 Modulation depth $\Delta T/T$ of racetracks with different numbers of nanoantennas, direct modulation. Direct-modulation amplitudes $\Delta T/T$ of top (a) and bottom (b) outputs from five racetracks which have the nanoantenna arrays with element numbers from 0 to 5. Six resonant modes are included, in which odd modes and even modes are grouped in green and red shapes, respectively. The insets show the SEM images of the nanoantennas on the racetrack around position $-L/4$ (dashed line). Scale bar, 500 nm.

S4. Asymmetry of top and bottom outputs for the racetrack resonators with nanoantennas

Ideally, with the antennas positioned on symmetric points of the racetrack, the top and bottom outputs will be identical. However, we observed that they were different from each other obviously when measuring the output spectra with the CW tunable laser. Especially, for one racetrack, it usually has one output with a suppression of alternating peaks but the other one without (Fig. S8). Except the possible variation among output grating couplers, this asymmetry can be attributed to the position shift of the nanoantennas on the circulating path of the resonant waves, which is reproduced in our simulation with Lumerical FDTD. In the simulation we shift bottom group of antenna along the waveguide by -50 nm to 50 nm on a 3-antenna racetrack. As shown in Fig. S9, when the antenna array is moved away from the symmetric point, the contrast between the unperturbed and suppressed resonances increases for one drop output but decreases for the other output. Experimentally the shift can happen with fabrication inaccuracy, which had probably caused the observed asymmetry. This behaviour is believed to be relevant to the intermediate-phase-shift induced asymmetry mentioned in the main text when the standing wave nodes (or anti-nodes) are not aligned with the antennas.

We had also designed a variety of incoupling gaps between the bus waveguides and racetracks to locate the critical coupling. The racetracks with 4- and 5-antenna arrays are in the over-coupling regime, leading to lower quality factors and thus larger widths of the resonances (Fig. S8d and S8e).

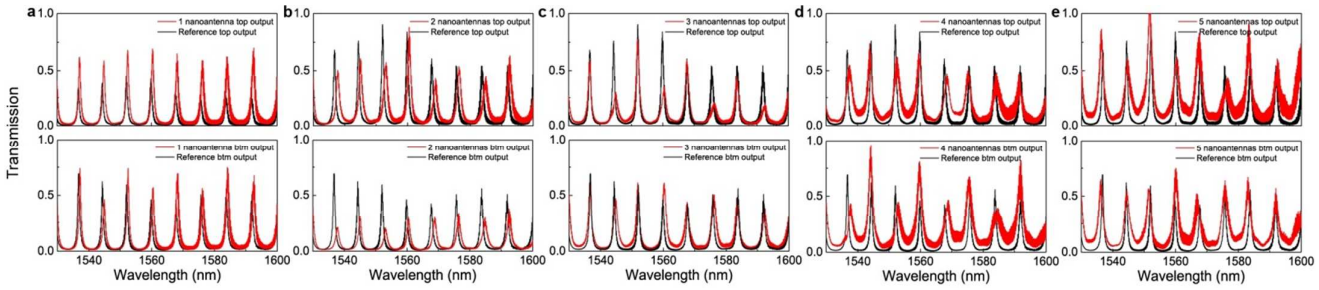

Figure S7 a-e Transmission spectra of top and bottom outputs., Top (upper row) and bottom (lower row) output spectra of the racetrack resonators with 1-5 nanoantennas, respectively.

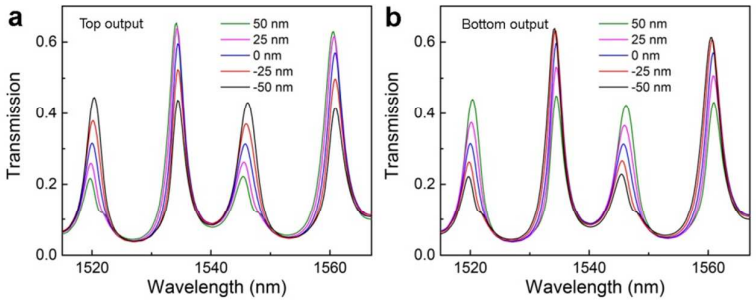

Figure S8 Effect of antenna positioning error. a and **b,** Simulated top and bottom output spectra from a racetrack resonator with 3-antenna arrays, respectively. The position of the antenna array on the bottom is shifted along the waveguide by -50 nm to 50 nm.

S5. Simulated near field of nanoantennas on racetrack resonator for an odd mode

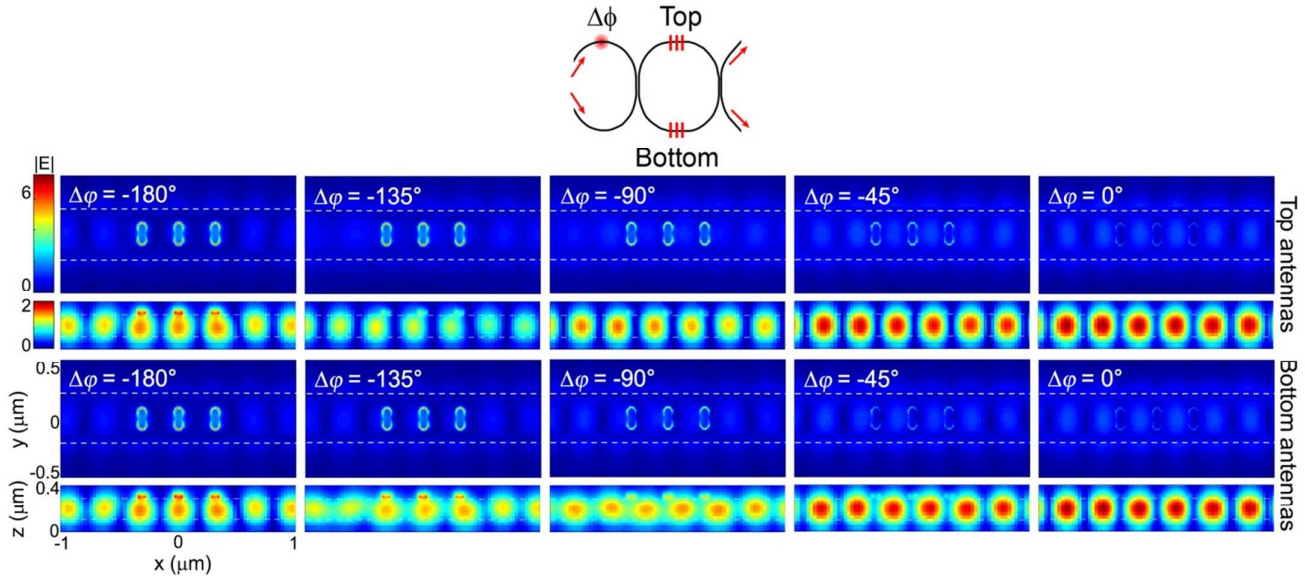

Figure S9 Simulated near-field maps. Simulated electric field magnitude distributions for top (middle row) and bottom (bottom row) groups of nanoantennas dependent on the top input phase (-180° to 0° from left column to right column). White dashed lines outline the edges of the waveguide. The wavelength is at 1547 nm which is located around an odd mode of the racetrack. The top illustration gives the schematic of the racetrack resonator with 3-antenna groups on the top and bottom sections of the racetrack. Phase change $\Delta\varphi$ on the top input is also indicated.